

Nonlinear dynamic analysis of SWNTs conveying fluid using nonlocal continuum theory

Seyed Ali Hosseini Kordkheili^{*1}, Taha Mousavi^{1a} and Hamid Bahai^{2b}

¹Aerospace Engineering Department, Sharif University of Technology, Azadi Ave., Tehran, Iran

²School of Engineering and Design, Brunel University, Uxbridge, UB8 3PH, London, U.K.

(Received May 16, 2017, Revised February 25, 2018, Accepted March 15, 2018)

Abstract. By employing the nonlocal continuum field theory of Eringen and Von Karman nonlinear strains, this paper presents an analytical model for linear and nonlinear dynamics analysis of single-walled carbon nanotubes (SWNTs) conveying fluid with different boundary conditions. In the linear analysis the natural frequencies and critical flow velocities of SWNTs are computed. However, in the nonlinear analysis the effect of nonlocal parameter on nonlinear dynamics of cantilevered SWNTs conveying fluid is investigated by using bifurcation diagram, phase plane and Poincare map. Numerical results confirm existence of chaos as well as a period-doubling transition to chaos.

Keywords: fluid conveying single-walled carbon nanotube; nonlocal continuum field theory; Von Karman nonlinear strain; chaos

1. Introduction

Recently researchers have become increasingly interested in studying nonlocal and van der Waals (vdW) force effects on dynamic behavior of carbon nanotubes (CNTs) (Bagdatli 2015, Tufekci *et al.* 2016 and Kaghazian *et al.* 2017). The first study on vibration and instability of CNTs conveying fluid was apparently carried out by Yoon *et al.* (2005). Subsequently, there have been a number of further studies on the topic conducted by other researchers. Khosravian and Rafii-Tabar (2007) studied the flow of viscous fluids through multi-walled carbon nanotubes (MWNTs) without considering nonlocal effect. They found that nanotubes conveying viscous fluids are more stable against vibration-induced buckling than nanotubes conveying non-viscous fluids, and that the aspect ratio plays the same role in both cases. Lee and Chang (2009) also studied vibration of a clamped-clamped SWNTs conveying viscous fluid using a nonlocal elastic model. They found that under the same velocity conditions, increasing the viscous parameter, aspect ratio or elastic medium constant increases the frequency of SWNTs. Wang and Ni (2009) found that during the flow of a fluid through a nanotube, modelled as a continuum beam, the effect of viscosity of the flowing fluid on vibration and instability of CNTs may be ignored. Later on, in order to consider the effect of the geometric nonlinearity on the transverse vibration of the double-walled carbon nanotubes (DWNTs) conveying fluid, Kuang *et al.* (2009) employed a nonlinear vdW force model without considering the nonlocal effect. The study showed

that the effect of geometric nonlinearity on the amplitude-frequency properties can be neglected.

Both Timoshenko and Euler-Bernoulli (EB) beam theories have been used by researchers to model flow of a non-viscous fluid in CNTs. In the absence of nonlocal effects, Khosravian and Rafii-Tabar (2008) found that the Timoshenko beam theory predicts the loss of stability at lower fluid flow velocities, a phenomenon which is neglected when using the EB classical beam theory. By considering nonlocal effects, Wang (2009a) studied dynamic behavior of DWNTs conveying fluid and found that their natural frequencies depended on nonlocal parameters. Ke and Wang (2011) also studied flow-induced vibration and instability of embedded DWNTs based on a modified coupled stress and the Timoshenko beam theory. They found that the critical flow velocity of the DWNTs increases with an increase in the length scale parameter and DWNTs with larger aspect ratio is more likely to cause divergence instability. A number of studies have been also conducted on vibration and instability of cantilevered CNTs conveying fluid (Yoon *et al.* 2006, Wang 2009b, Sobamowo 2016). Among these, only Wang (2009b) considered nonlocal effect on cantilevered CNTs conveying fluid. He has shown that nonlocal parameter (e) effects may be neglected for micro-beams. However according to our results reported in the present work, the results of Wang's paper are not representative for cantilevered systems with $e > 0$.

DWNTs conveying fluid have been also modeled based on Donnell's shell theory (Chang and Liu 2011). It is noted that when the length of DWNTs decreases, a comparative difference between the results from Eulerian beam and Donnell's shell models appears. Also, it is revealed that as the flow velocity increases, DWNTs have a way to get through multi-bifurcations of the first (pitchfork) and second (Hamiltonian Hopf) bifurcations in turn (Chang and

*Corresponding author, Associate Professor

E-mail: ali.hosseini@sharif.edu

^aM.Sc. Student

^bProfessor

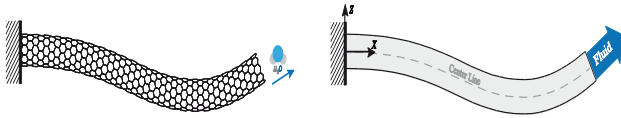


Fig. 1 A Continuum model of a nanotube conveying fluid

Liu 2011). Chemi *et al.* (2018) employed nonlocal Timoshenko beam theory to study buckling behavior of chiral double-walled carbon nanotubes embedded in an elastic medium.

This paper aims to study nonlinear dynamics behavior of SWNTs conveying fluid with different boundary conditions in present of small scale effects. For this purpose, the nonlocal continuum field theory of Eringen together with Von Karman nonlinear strains are employed to develop an analytical model for the problem. Numerical results on chaos and a period-doubling transition to chaos are presented.

2. Nonlinear nonlocal formulation for bending of Euler-Bernoulli beam theory

Reddy (2010) reformulated classical and shear deformation beam and plate theories using Eringen (2002) nonlocal elasticity theory. Also, Wang (2009b) presented a nonlocal Euler-Bernoulli elastic beam model for the vibration and instability of pipes conveying fluid using the theory of nonlocal elasticity. For the sake of completeness, we have presented formulation here which also includes our correction to the beam theory formulation.

2.1 Euler-Bernoulli beam theory (EBT)

The displacement field in EBT is given by

$$u_1(x, z) = u(x) - z \frac{dw}{dx}, \quad u_2 = 0, \quad u_3 = w(x) \quad (1)$$

where u and w are the axial and transverse displacement of points on center line ($z=0$) of nanotube in Fig. 1. Von Karman nonlinear strain for EBT is considered as follows

$$\varepsilon_{xx} = \frac{du}{dx} + \frac{1}{2} \left(\frac{dw}{dx} \right)^2 - z \frac{d^2w}{dx^2} = \bar{\varepsilon} + z\bar{\varepsilon} \quad (2)$$

Now using the principal of virtual displacement we have

$$\int_0^l (+f\delta u + q\delta w - N\delta\bar{\varepsilon} - M\delta\bar{\varepsilon}) dx = 0 \quad (3)$$

where $f(x)$ and $q(x)$ are the axial and transverse distributed forces (measured per unit un-deformed length). N and M are also the stress resultants, i.e.,

$$N = \int_A \sigma_{xx} dA, \quad M = \int_A z\sigma_{xx} dA \quad (4)$$

By using the principal of virtual displacement, we obtain the following Euler-Lagrange equations in $0 < x < 1$

$$\frac{dN}{dx} + f = 0 \quad (5)$$

$$\frac{d^2M}{dx^2} + \frac{d}{dx} \left(N \frac{dw}{dx} \right) + q = 0 \quad (6)$$

The boundary conditions involve specifying one element of each of the following three pairs at $x=0$ and $x=1$

$$\begin{aligned} &u \text{ or } N \\ &w \text{ or } V \equiv \frac{dM}{dx} + N \frac{dw}{dx} \\ &\frac{dw}{dx} \text{ or } M \end{aligned} \quad (7)$$

Here, V denotes the equivalent shear force. Reddy (2010) reported Eqs. (6) and (7) in the following incorrect form

$$\frac{d^2M}{dx^2} - \frac{d}{dx} \left(N \frac{dw}{dx} \right) + q = 0 \quad (8)$$

$$V \equiv \frac{dM}{dx} - N \frac{dw}{dx} \quad (9)$$

2.2 Nonlocal theory

Equivalent differential form of the constitutive relations in nonlocal theory (Eringen 2002) is,

$$(1 - \mu \nabla^2) \sigma_{ij} = C_{ijmn} \varepsilon_{mn}, \quad \mu = e_0^2 a^2 \quad (10)$$

where e_0 is a material constant, and a is the internal characteristic length. By ignoring nonlocal effect in the thickness direction, Relation (10) takes the following form for homogeneous isotropic Euler-Bernoulli beams,

$$\Pi(\sigma_{xx}) = E\varepsilon_{xx}, \quad \Pi = 1 - \mu \frac{d^2}{dx^2} \quad (11)$$

where E is Young's modulus and Π is a linear operator.

2.3 Constitutive relations

Constitutive relations are

$$\Pi(N) = EA\bar{\varepsilon} \quad (12)$$

$$\Pi(M) = EI\bar{\varepsilon} \quad (13)$$

where I is second moment of area about the y -axis and

$$A = \int_A dA, \quad \int_A z dA = 0 \quad (14)$$

2.4 Stress resultant in term of displacements

Substituting for the first derivative of the axial force N from Eq. (5) into Eq. (12), we obtain,

$$N = EA\bar{\varepsilon} - \mu \frac{df}{dx} \tag{15}$$

Also, substituting for the second derivative of M from Eq. (6) into Eq. (13), we obtain,

$$M = EI\bar{\varepsilon} - \mu \left(\frac{d}{dx} \left(N \frac{dw}{dx} \right) \right) - \mu q \tag{16}$$

where N is given by Eq. (15).

2.5 Equilibrium equations

Substituting N from Eq. (15) into Eq. (5), and substituting M from Eq. (16) into Eq. (6), we obtain equilibrium equations as follows

$$\frac{d}{dx} (EA\bar{\varepsilon}) + \Pi(f) = 0 \tag{17}$$

$$\frac{d^2}{dx^2} (EI\bar{\varepsilon}) + \Pi \left(\frac{d}{dx} \left(N \frac{dw}{dx} \right) \right) + \Pi(q) = 0 \tag{18}$$

where N is given by Eq. (15). Conventional Euler-Bernoulli beam theory is obtained by setting $m=0$ and $P=1$ in Eq. (17) and Eq. (18).

2.6 Fluid force model

Non-viscous fluid flow in a pipe whose diameter is sufficiently smaller than its length (slender body) can be modelled as a plug flow as follows (Paidoussis 1998)

$$q(x) = m_f v^2 w'' + 2m_f v \dot{w}' + (m_f + m_n) \ddot{w} \tag{19}$$

where $q(x)$ is transverse force on nanotube and other three terms in the right hand side of the equation are related to centrifugal, coriolis and inertia forces, respectively. Also, v is the mean flow velocity and m_n and m_f are the mass per unit length of the nanotube and fluid, respectively. The dot and prime denote derivatives with respect to the time t and axial coordinate x , respectively.

2.7 The governing equation

By ignoring axial force and displacement in Eq. (15) we obtain

$$N = \frac{1}{2} EA \left(\frac{\partial w}{\partial x} \right)^2 \tag{20}$$

After substituting Eqs. (19) and (20) into Eq. (18), the governing equilibrium equation is obtained as follows

$$EIw^{(4)} - EA \left[\frac{3}{2} w'^2 w'' - \mu \left(\frac{3}{2} w^{(4)} w'^2 + 3w''^3 + 9w''' w'' w' \right) \right] + \Pi \left(m_f v^2 w'' + 2m_f v \dot{w}' + (m_f + m_n) \ddot{w} \right) = 0 \tag{21}$$

Eq. (21) can also be express in following form

$$EIw^{(4)} - EA \Pi \left(\frac{3}{2} w'' (w')^2 \right) + \Pi \left(m_f v^2 w'' + 2m_f v \dot{w}' + (m_f + m_n) \ddot{w} \right) = 0 \tag{22}$$

The boundary conditions involve specifying one element of each of the following pairs at $x=0$ and $x=l$

$$\begin{aligned} w' \text{ or } M &\equiv -EIw'' - \frac{3}{2} \mu EA w'^2 w'' - \mu q(x) \\ w \text{ or } V &\equiv -EIw''' - \frac{3}{2} \mu EA (2w' w''^2 + w'^2 w''') \\ &\quad - \mu \frac{d}{dx} q(x) + \frac{1}{2} EA w'^3 \end{aligned} \tag{23}$$

Now, introducing the following dimensionless quantities

$$\begin{aligned} \eta = \frac{w}{l}, \xi = \frac{x}{l}, \beta = \frac{m_f}{m_f + m_n}, \tau = \left(\frac{EI}{m_f + m_n} \right)^{1/2} \frac{t}{l^2} \\ e^2 = \frac{\mu}{l^2}, u = \left(\frac{m_f}{EI} \right)^{1/2} vl, \delta = \frac{l^2 A}{I}, \Omega = 1 - e^2 \frac{\partial^2}{\partial \zeta^2} \end{aligned} \tag{24}$$

Dimensionless form of Eq. (22) can be expressed as follows

$$\eta^{(4)} - \frac{3}{2} \delta \Omega \left(\eta'' (\eta')^2 \right) + \Omega \left(u^2 \eta'' + 2u \sqrt{\beta} \dot{\eta}' + \ddot{\eta} \right) = 0 \tag{25}$$

and dimensionless form of boundary conditions (23) are

$$\begin{aligned} \eta' \text{ or } \bar{M} &\equiv -\eta'' - \frac{3}{2} e^2 \delta (\eta')^2 \eta'' - e^2 (\bar{q}) \\ \eta \text{ or } \bar{V} &\equiv -\eta''' - \frac{3}{2} e^2 \delta \left(2\eta' (\eta'')^2 + (\eta')^2 \eta''' \right) \\ &\quad - e^2 \frac{d}{d\xi} (\bar{q}) + \frac{1}{2} \delta (\eta')^3 \end{aligned} \tag{26}$$

where $\bar{q} = u^2 \eta'' + 2u \sqrt{\beta} \dot{\eta}' + \ddot{\eta}$. The dot and prime denote derivatives with respect to the dimensionless time τ and dimensionless axial coordinate ζ , respectively. Wang (2009b) presented boundary conditions as follows:

- pinned-pinned (PP)

$$\eta''(0, \tau) = \eta(0, \tau) = 0, \eta''(1, \tau) = \eta(1, \tau) = 0 \tag{27}$$

- clamped-clamped (CC)

$$0 = (\tau, l) \eta = (\tau, l) \eta', 0 = (\tau, 0) \eta = (\tau, 0) \eta' \tag{28}$$

- clamped-free (CF)

$$\eta'(0, \tau) = \eta(0, \tau) = 0, \eta''(1, \tau) = \eta'''(1, \tau) = 0 \tag{29}$$

It appears that in Wang’s paper (2009b) the derivatives with respect to the dimensionless time τ have been omitted. When using the formulation reported by Wang (2009b),

different results are obtained in comparison to those reported in that paper. This could possibly be due a programming error.

3. Solution methods

3.1 Differential quadrature (DQ) method

DQ method was first introduced by Richard Bellman and his associates in the early 1970s and since then some books have been written on the method by various authors, e.g., Shu (2000), Chen (2006) and Zhi (2009). The DQ method is widely used in the analysis of nanotube conveying fluid problems (Wang *et al.* 2008, Wang 2009b and Zhen and Fang 2010). In the linear analysis we employed DQ method to compare our results with those reported by Wang (2009b). The basic premise of the DQ method is that the derivative of a function at a sample point is approximated by the weighed linear sum of the function's value at all of the sample points in the problem domain. Hence, w and its k^{th} derivative with respect to x can be approximated by

$$\left. \frac{d^k \eta}{dx^k} \right|_{x=x_i} = \sum_{j=1}^N C_{ij}^{(k)} \eta(x_j) \tag{30}$$

where $x_j=1,2,\dots,N$ are discrete point and $C_{ij}^{(k)}$ is weighed coefficients whose definitions can be found in Zhen, B. Fang (2010). In this study, the grid points are chosen as Chebyshev-Gauss-Lobatto pattern (Shu 2000)

$$x(i) = \frac{1}{2} \left(1 - \cos \left(\pi \frac{i-1}{N-1} \right) \right), \quad i = 1, 2, \dots, N \tag{31}$$

By utilizing the DQ method, we can discretize spatial derivative and obtain a set of nonlinear ordinary differential equations which can be expressed in matrix form as

$$\mathbf{M}\{\ddot{\eta}\} + \mathbf{C}\{\dot{\eta}\} + (\mathbf{K}_L + \mathbf{K}_{NL})\{\eta\} = 0 \tag{32}$$

where \mathbf{M} is mass matrix and \mathbf{K}_L is the linear stiffness matrix. \mathbf{K}_{NL} is nonlinear stiffness matrix which is function of η and \mathbf{C} is the damping matrix. For the linear analysis by ignoring \mathbf{K}_{NL} the solution of Eq. (32) can be written in the form of

$$\{\eta\} = \{\bar{\eta}\} \exp(\omega\tau) \tag{33}$$

where $\{\bar{\eta}\}$ is an undetermined function of vibration amplitude, $Im(\omega)$ is natural frequency and $Re(\omega)$ is related to system damping. Substituting Eq. (33) into Eq. (32) we obtain the following eigenvalue problem,

$$(\mathbf{M}\omega^2 + \mathbf{C}\omega + \mathbf{K}_L)\{\bar{\eta}\} = 0 \tag{34}$$

3.2 Galerkin method

By employing Galerkin procedure, we can project

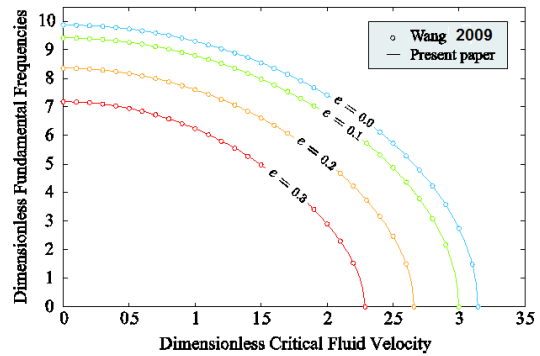


Fig. 2 Fundamental frequencies for various nonlocal parameter and fluid velocity of a PP system

nonlinear PDE into a finite set of nonlinear coupled ODEs. The solution of Eq. (25) can be written in the form

$$\eta(\xi, \tau) = \sum_{i=1}^N \phi_i(\xi) q_i(\tau) \tag{35}$$

where $\phi_i(\xi)$ is i^{th} Eigen function of a cantilevered beam. Substituting (35) in Eq. (25), multiplying it by $\phi_j(\xi)$ and integrating with respect to ξ along $[0,1]$ we obtain

$$M_{ij} \ddot{q}_j + C_{ij} \dot{q}_j + K_{ij} q_j + \alpha_{ijkl} q_j q_k q_l = 0 \tag{36}$$

where

$$\begin{aligned} M_{ij} &= \delta_{ij} - e^2 \int_0^1 \phi_j \phi_j'' d\xi \\ C_{ij} &= 2u\sqrt{\beta} \int_0^1 \phi_i \phi_j' - e^2 \phi_j''' d\xi \\ K_{ij} &= \int_0^1 \phi_i \phi_j^4 + u^2 \phi_j'' - e^2 u^2 \phi_j^4 d\xi \\ \alpha_{ijkl} &= 3\delta \int_0^1 \phi_i \left(-\frac{1}{2} \phi_j' \phi_k' \phi_l'' + \frac{1}{2} e^2 \phi_j^4 \phi_k' \phi_l' \right. \\ &\quad \left. + e^2 \phi_j'' \phi_k'' \phi_l'' + 3e^2 \phi_j''' \phi_k'' \phi_l' \right) d\xi \end{aligned} \tag{37}$$

This finite set of ODEs can capture essential system behaviour if we choose appropriate and sufficient number of eigen functions. The number of eigen functions can be dictated by some of the parameters in PDE. Paidoussis (1998) studied critical flow velocity versus mass ratio for a cantilevered pipe conveying fluid. He showed that results are sensitive to number of modes and indeed as $\beta \rightarrow 1$ more and more beam modes participate in the dynamic behavior of the pipe.

4. Results

4.1 Linear analysis

Pipes supported at both ends lose stability via divergence and cantilevered pipes lose stability via flutter. As the dynamics of these systems are fundamentally different, they will be studied separately. Here, again we use mass ratio $\beta=0.64$ as used by Wang (2009b) in order to compare our linear analysis results with those reported in his paper. However, the main results are reported for $\beta=0.1$,

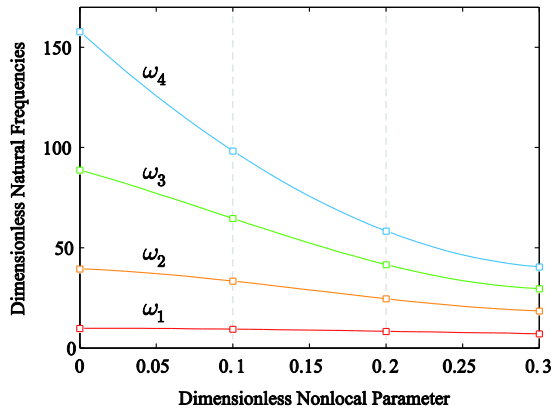


Fig. 3 Four natural frequency of a PP system for $\beta=0.64$ and various nonlocal parameter values at $u=0$

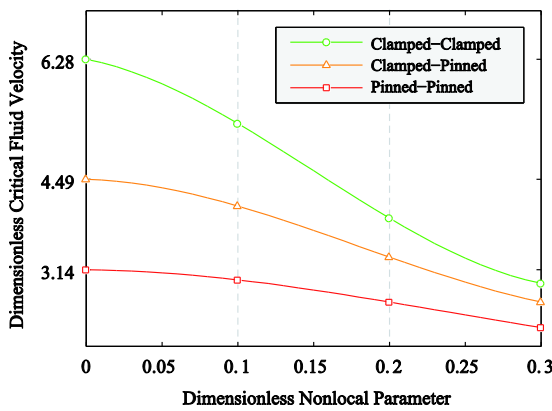


Fig. 4 Critical fluid velocity of different supported systems and nonlocal parameters values

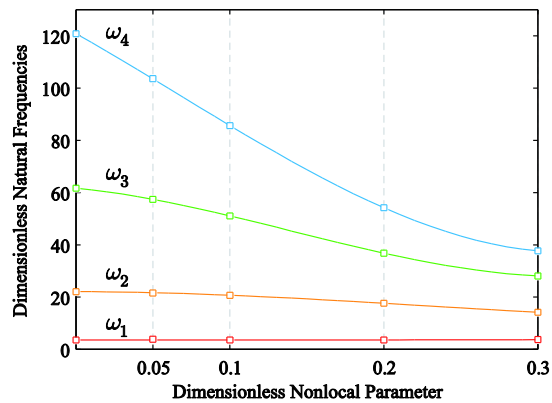


Fig. 5 Four natural frequencies of a cantilevered system for $\beta=0.64$ and various nonlocal parameter at $u=0$

which is more realistic for SWNTs (Lee and Chang 2009). Also, in this section the correct results for cantilevered pipes are presented.

4.1.1 Both end supported systems

In this section in order to study boundary condition effects on dynamical behavior clamped-clamped (CC), clamped-pinned (CP) and pinned-pinned (PP) boundary conditions are considered. Fig. 2 shows the dimensionless fundamental frequency as a function of dimensionless flow

velocity for a PP system.

As can be seen in this figure, increasing the nonlocal parameter decreases both fundamental frequency value and their respective critical flow velocity. According to this figure, the results from linear solution of the presented formulation and those from Wang (2009b) are entirely consistent. Fig. 3 shows the first four dimensionless natural frequencies of the PP system for $\beta=0.64$ and various e values at $u=0$. As seen in this figure increasing the nonlocal parameter causes natural frequencies to become closer to each other with a more pronounced effect in higher frequency range.

Fig. 4 shows critical flow velocity (divergence velocity) for different boundary conditions and different nonlocal parameters. From this figure it can be seen that critical flow velocities are generally decreased with increasing values of nonlocal parameter.

4.1.2 Cantilevered system

In this section results are presented for cantilevered system with mass ratio $\beta=0.64$, the same value considered by Wang (2009b). Fig. 5 shows the first four natural frequencies of a cantilevered system for $\beta=0.64$ and various e values at $u=0$.

As in the case of the PP system (Fig. 3), it is seen that increasing nonlocal parameter, decreases natural frequencies with a more significant effect in the higher frequency range. Fig. 6 shows eigenvalue evolution in Argand diagram with increasing flow velocity for $e=0,0.05,0.1$ and $\beta=0.64$. Circle marks in these figures show eigenvalues for flow velocity equal zero and square marks show eigenvalues for critical flow velocity. According to the results, in the case of $\beta=0.64$ and $e=0$ (Fig. 6(d)) Hopf bifurcation occurs via first mode at $u_c=10.32$ (same as Fig. 4 in Wang 2009b).

But unlike Wang's results in the case of $\beta=0.64$ and $e=0.1$, instability occurs in $u_c=8.35$ via first mode (Fig. 6(e)) and not in $u_c=3.32$ via second mode (Fig. 5 in Wang 2009b). Also, there is no third mode oscillatory instability via another Hopf bifurcation. In the case of $e=0.05$ and $\beta=0.64$, the system loses its stability at $u_c=10.64$. Therefore, unlike PP systems, increasing nonlocal parameter do not generally decrease the critical flow velocity. In the case of $\beta=0.1$ and $e=0,0.05,0.1$ Hopf bifurcation occurs at $u_c=4.75,4.61,4.24$ respectively and via second mode. As seen in Fig. 6, nonlocal parameter has more effect on critical flow velocity and eigenvalues evolution of system at higher mass ratios b .

4.2 Nonlinear analysis

4.2.1 Bifurcation diagram

Bifurcation diagrams show dynamic behavior evolution of a system by varying a system parameter whilst keeping others fixed. Fig. 7 shows bifurcation diagrams for various nonlocal parameters by changing fluid velocity. In these figures, the displacements of the nanotube's free-end $\eta(1,\tau)$ are plotted whenever its velocity $\dot{\eta}(1,\tau)$ becomes zero. Since in some range of values of u the symmetry of the solution was violated, we utilized both positive and negative initial conditions in the calculations

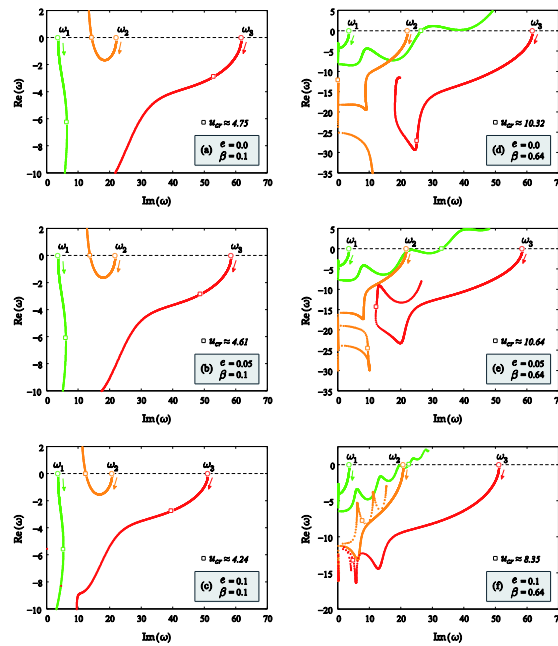


Fig. 6 Eigenvalues evolution of a cantilevered system with various u for $e=0,0.05,0.1$ and $\beta=0.64$

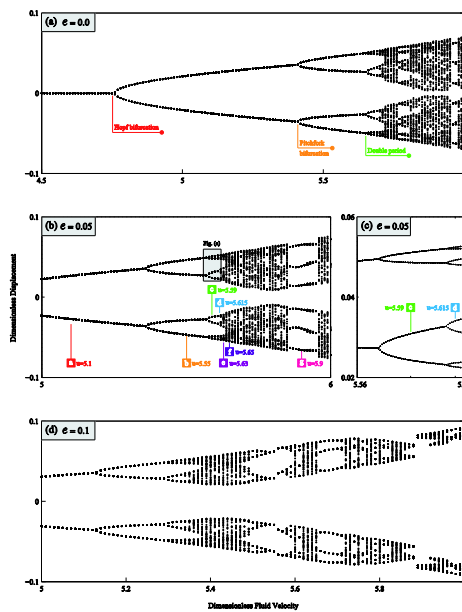


Fig. 7 Bifurcation diagrams at nanotube free-end point $h=(1,t)$ for different nonlocal parameters

$$\begin{aligned}
 q_1(0) &= \pm 0.05 & q_2(0) &= q_3(0) = 0 \\
 \dot{q}_1(0) &= \dot{q}_2(0) = \dot{q}_3(0) = 0
 \end{aligned}
 \tag{38}$$

For the sake of clarification in the results, the transient solutions were discarded. As seen in Fig. 7(a), for small value of u (before Hopf bifurcation) the system is at a stable fixed point and any disturbance around it will converge the system to its original stable position. Following the Hopf bifurcation ($u:4.752$), the system undergoes symmetric limit cycle. The radius of the limit cycle raises as fluid velocity increases. Thereafter, the system loses its symmetry and symmetric limit cycle is replaced by an asymmetric cycle, which corresponds to the pitchfork bifurcation. Fig. 7(c)

shows the bifurcation diagram for a smaller range of u , where a period-doubling bifurcation is visible. This is then followed by occurrence of chaotic motion. Obviously, the route to chaos for different nonlocal parameter is via a period-doubling motion. It is interesting to note that after chaotic motion, in some range of u , periodic-motion prevails in the system (e.g., Fig. 8(g) shows 3-period motion) after which the system becomes chaotic again.

4.2.2 Phase-plane and time history diagrams

It is instructive to look at phase-plane corresponding to different fluid velocity which is marked in bifurcation diagrams (Fig. 7(a)-(g)). The middle column in Fig. 8 shows Phase plane for different fluid velocities. For the purpose of constructing phase plane diagrams,

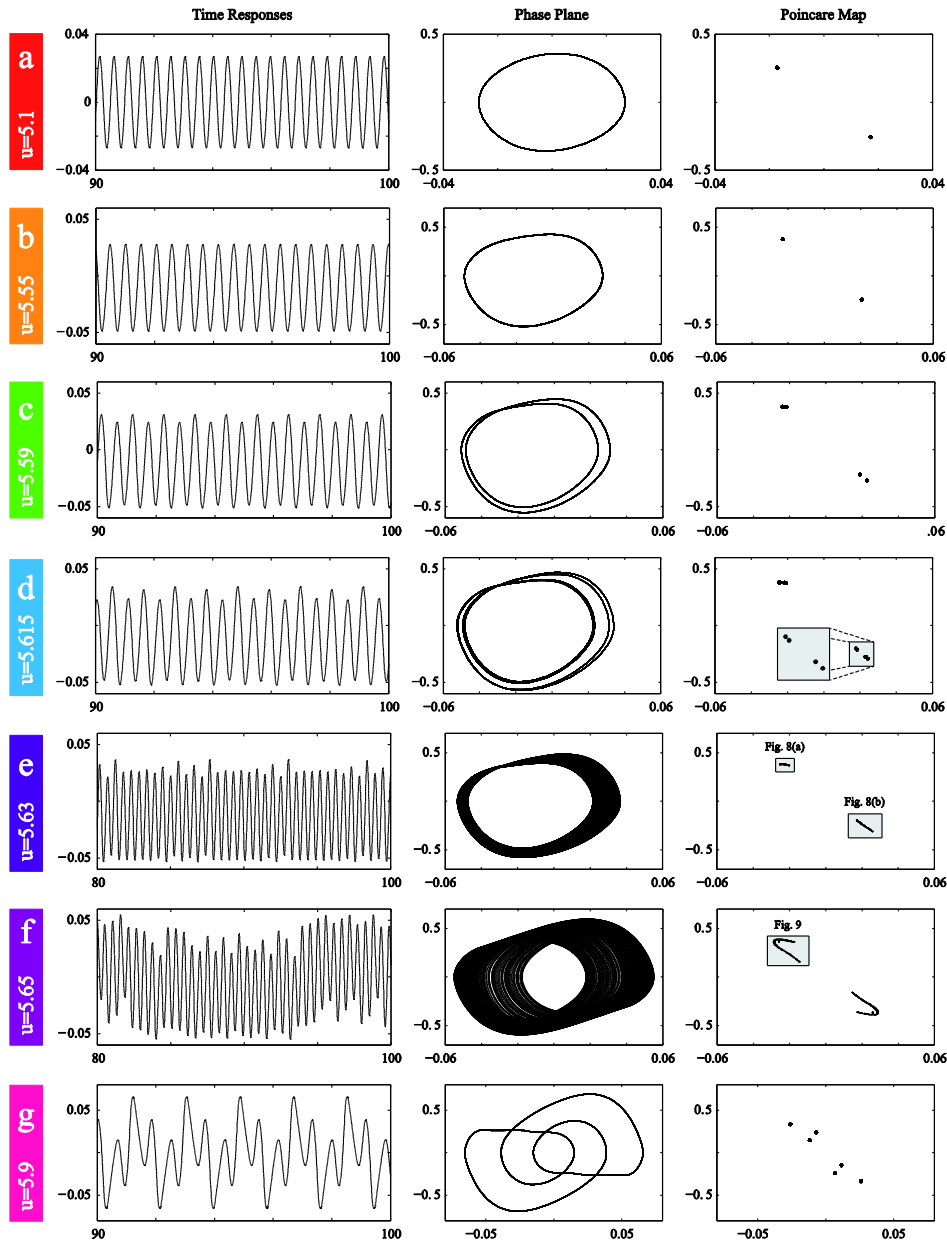


Fig. 8 Time responses, phase planes and Poincaré maps for reference points in Fig. 7

dimensionless displacement against dimensionless velocity at nanotube free-end $\eta(1, \tau)$ is plotted. As mentioned previously, for small values of u , the system is at a stable fixed point. As velocity increases, the system undergoes symmetric limit cycle (a), asymmetric limit cycle (b), period-2 motion (c), period-4 motion (d), an asymmetric narrow-band chaotic motion (e) and a wide-band chaotic motion (f). Therefore, the sequence to chaos is via the period-doubling motion. Left column in Fig. 8 show corresponding time history of phase planes.

4.2.3 Poincaré maps

The Poincaré map is a powerful technique for distinguishing chaotic responses from Periodic ones or random noise. For an autonomous system, there are many ways to construct Poincaré map. The scheme selected here

is to plot displacement and velocity at nanotube free-end $\eta(1, \tau)$, when displacement of another point of nanotube (e.g., $h=(0.7, t)$) is zero (Paidoussis *et al.* 1989). Right column in Figs. 8 show Poincaré maps. Figs. 8(a)-(d) and Fig. 8(g) show periodic motions. When the motion is periodic, Poincaré map should consist of twice the number of period points. (e.g., there are 8 point in Fig. 8(d) which correspond to period-4 motion). Figs. 8(e) and 8(f) shows narrow and wide-band chaotic motions. Also, Figs. 9 and 10 show a refined Poincaré map for these chaotic motion. As seen in these figures when the motion is chaotic, Poincaré map consist of infinite number of points but has a very definite structure in contrast to random noise motion in which the points fill the map.

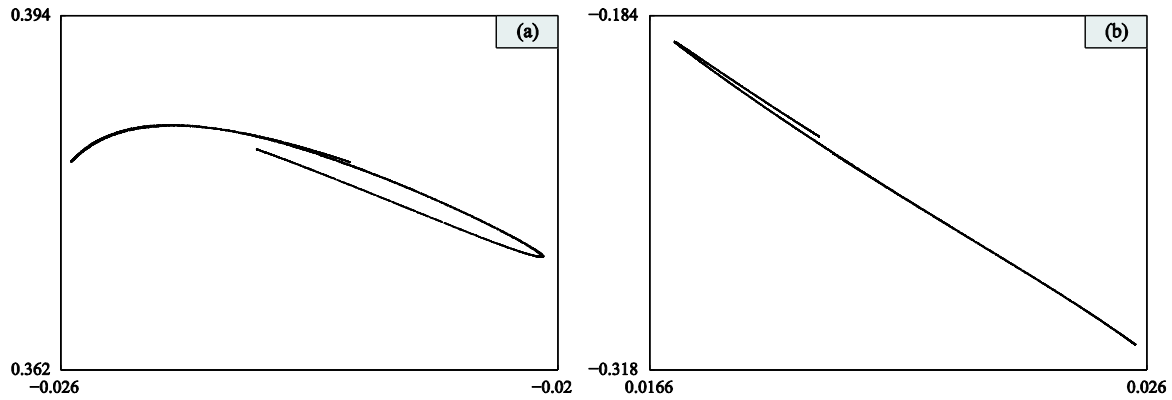


Fig. 9 Detailed Poincare map for point (e) in Fig. 7 correspond to narrow-band chaotic motion

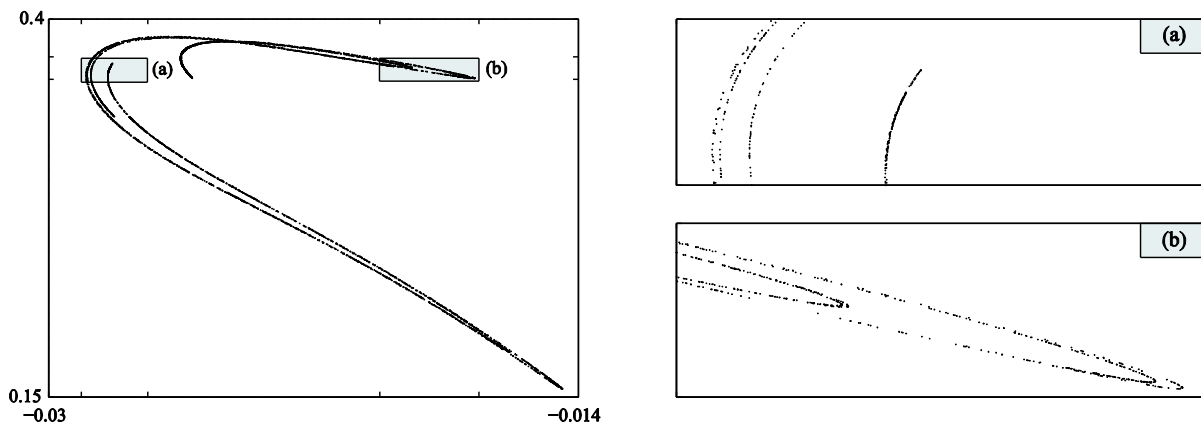


Fig. 10 Detailed Poincare map for point (f) in Fig. 7 correspond to wide-band chaotic motion

5. Conclusions

An analytical model of a SWNTs conveying fluid has been developed by employing nonlocal continuum and considering Von Karman nonlinear geometry. In the linear analysis, which has been carried out by DQ method, the natural frequencies and critical flow velocities are discussed. The results show that:

- Increasing nonlocal parameter of both supported ends and cantilevered system, causes its natural frequencies to be shifted closer to each other and have more influence in the higher frequency range.
- Critical fluid velocity for different two end supported systems decrease as nonlocal parameter increase.
- Unlike two supported systems, increasing nonlocal parameter generally do not decrease critical flow velocity in the cantilevered beams.
- Nonlocal parameter has more effect on critical flow velocity and eigenvalues of a system with higher mass ratio b .

Nonlinear analysis has been carried out by bifurcation diagrams, phase plane and Poincare map. Bifurcation diagram for different nonlocal parameters with the flow velocity as a parameter shows chaotic motion in some range of flow velocity. The results demonstrate that:

- A period-doubling bifurcation to chaos occurs for all the considered nonlocal parameters.
- Increasing nonlocal parameter can cause the band of oscillation to get narrower in the chaotic region.

Period-doubling transition to chaos are discussed by time history, phase plane and Poincare map.

References

- Bagdatli, S.M. (2015), "Non-linear transverse vibrations of tensioned nanobeams using nonlocal beam theory", *Struct. Eng. Mech.*, **55**(2), 281-298.
- Chang, T. and Liu, M. (2011), "Flow-induced instability of double-walled carbon nanotubes based on nonlocal elasticity theory", *Phys. E: Low-Dimens. Syst. Nanostruct.*, **43**(8), 1419-1426.
- Chen, C. (2006), *Discrete Element Analysis Methods of Generic Differential Quadratures*, Springer-Verlag Berlin Heidelberg.
- Chemi, A., Zidour, M., Heireche, H., Akrak, K. and Bousahla, A.A. (2018), "Critical buckling load of chiral double-walled carbon nanotubes embedded in an elastic medium", *Mech. Compos. Mater.*, 1-10.
- Eringen, A. (2002), *Nonlocal Continuum Field Theories*, New York, Springer-Verlag.
- Kaghazian, A., Hajnayeb, A. and Foruzande, H. (2017), "Free vibration analysis of a piezoelectric nanobeam using nonlocal elasticity theory", *Struct. Eng. Mech.*, **61**(5), 617-624.
- Ke, L. and Wang, Y. (2011), "Flow-induced vibration and instability of embedded double-walled carbon nanotubes based on a modified couple stress theory", *Phys. E: Low-Dimens. Syst. Nanostruct.*, **43**(5), 1031-1039.
- Khosravian, N. and Rafii-Tabar, H. (2007), "Computational modelling of the flow of viscous fluids in carbon nanotubes", *J. Phys. D: Appl. Phys.*, **40**(22), 7046-7052.
- Khosravian, N. and Rafii-Tabar, H. (2008), "Computational

- modelling of a non-viscous fluid flow in a multi-walled carbon nanotube modelled as a Timoshenko beam”, *Nanotechnol.*, **19**(27), 275703.
- Kuang, Y., He, X., Chen, C. and Li, G. (2009), “Analysis of nonlinear vibrations of double-walled carbon nanotubes conveying fluid”, *Comput. Mater. Sci.*, **45**(4), 875-880.
- Lee, H. and Chang, W. (2009), “Vibration analysis of a viscous-fluid-conveying single-walled carbon nanotube embedded in an elastic medium”, *Phys. E: Low-Dimens. Syst. Nanostruct.*, **41**(4), 529-532.
- Paidoussis, P. (1998), *Fluid-Structure Interactions: Slender Structures and Axial Flow*, Academic Press, London, U.K.
- Paidoussis, M., Li, G. and Moon, F. (1989), “Chaotic oscillations of the autonomous system of a constrained pipe conveying fluid”, *J. Sound Vibr.*, **135**(1), 1-19.
- Reddy, J. (2010), “Nonlocal nonlinear formulations for bending of classical and shear deformation theories of beams and plates”, *Int. J. Eng. Sci.*, **48**(11), 1507-1518.
- Shu, C. (2000), *Differential Quadrature and Its Application in Engineering*, Springer-Verlag London Limited.
- Sobamowo, G.M. (2016), “Nonlinear vibration analysis of single-walled carbon nanotube conveying fluid in slip boundary conditions using variational iterative method”, *J. Appl. Comput. Mech.*, **2**(4), 208-221.
- Tufekci, E., Aya, S.A. and Oldac, O. (2016), “A unified formulation for static behavior of nonlocal curved beams”, *Struct. Eng. Mech.*, **59**(3), 475-502.
- Wang, L. (2009a), “Dynamical behaviors of double-walled carbon nanotubes conveying fluid accounting for the role of small length scale”, *Comput. Mater. Sci.*, **45**(2), 584-588.
- Wang, L. (2009b), “Vibration and instability analysis of tubular nano- and micro-beams conveying fluid using nonlocal elastic theory”, *Phys. E: Low-Dimens. Syst. Nanostruct.*, **41**(10), 1835-1840.
- Wang, L. and Ni, Q. (2009), “A reappraisal of the computational modelling of carbon nanotubes conveying viscous fluid”, *Mech. Res. Commun.*, **36**(7), 833-837.
- Wang, L., Ni, Q., Li, M. and Qian, Q. (2008), “The thermal effect on vibration and instability of carbon nanotubes conveying fluid”, *Phys. E: Low-Dimens. Syst. Nanostruct.*, **40**(10), 3179-3182.
- Yoon, J., Ru, C. and Mioduchowski, A. (2005), “Vibration and instability of carbon nanotubes conveying fluid”, *Compos. Sci. Technol.*, **65**(9), 1326-1336.
- Yoon, J., Ru, C. and Mioduchowski, A. (2006), “Flow-induced flutter instability of cantilever carbon nanotubes”, *Int. J. Sol. Struct.*, **43**(11-12), 3337-3349.
- Zhen, Y. and Fang, B. (2010), “Thermal-mechanical and nonlocal elastic vibration of single-walled carbon nanotubes conveying fluid”, *Comput. Mater. Sci.*, **49**(2), 276-282.
- Zong, Z. and Zhang, Y. (2009), *Advanced Differential Quadrature Methods*, Chapman and Hall/CRC, Boca Raton, Florida, U.S.A.